

Cortical bone porosity visualization using mercury porosimetry intrusion data

CARDOSO, Antônio V.; OLIVEIRA, Walisson José; VAZ, G.J.O.

Laboratório de Reologia, Setor de Análises Químicas,
Fundação Centro Tecnológico de Minas Gerais (CETEC)
Av. José Candido da Silveira nº 2000, CEP 31170-000, Belo Horizonte (MG), Brasil.
e-mail: antonio.cardoso@cetec.br, walissonjose@yahoo.com.br, gjovaz@cetec.br.

ABSTRACT

Cortical bone porosity of bovine tibia samples has been investigated using the mercury intrusion porosimetry (MIP) technique. Cortical bone porosity range from 10 nm (caniculae) to 40 μm (Harvers canals), well in the measuring range region for the MIP technique. Samples from fresh bovine cortical bone were treated, dried and cut into $\sim (3 \times 1 \times 1)$ cm pieces. The aim of the work was twofold: 1- To investigate bone porosity structure and direction quantitatively; 2- To obtain tri-dimensional scientific visualization (SV) images of cortical bone porosity. The MIP experiments associated with SV seem to be a good tool for studies of bone loss mechanisms, bone porosity distribution and bone growth phenomena.

Keywords: bone porosity, mercury porosimetry, scientific visualization.

1 INTRODUCTION

Bone mass loss is one of worst health problems occurring with aged people. Consequences are higher porosity and decrease in bone mechanical strength. Fractures are frequent and might result in long resting times and eventually permanent physical disability. [1]

Where the porosity is located is still a matter of debate. Cowin [2] has classified cortical bone porosity in four types of porosity: a- vascular (VP); b- lacunae-caniculae (LCP); c- collagen-apatite (CAP); d- intertrabecular (ITP). Vascular porosity is the set of the Havers and Volkman canals with radius around 20 μm [3]. Lacunae-caniculae porosity is compound by caniculae and lacunae with average radius approximately 0.1 μm . Collagen-apatite porosity are empty spaces left between collagen fibers and apatite crystals. Intertrabecular porosity is spaces on the trabecula with dimensions larger than 1 mm. Here, we are concerned with micrometer (from 3 nm to 360 μm) porosities which, of course, do not include the intertrabecular porosity. Scientific visualization is a software tool for helping one to transform experimental data in numerical format on images instead of graphics [4]. Experimental data from MIP technique is specially suitable to such an exercise because a considerable amount of data concerning sample porosity can be obtained in one single experiment.

Mercury intrusion porosimetry (MIP) is a commercial characterization technique for the analyses of average open porosity, pore size distribution, etc; and is routinely used as a characterization technique for ceramics, metals and minerals [5, 6, 7]. The principles of porosity size using MIP are based on the fact that mercury is a non-wetting liquid and the diameter of the open pore can be associated with the applied pressure via the Washburn equation:

$$D = \frac{-4\gamma \cos \theta}{P} \quad (1)$$

Where D is the porous diameter, γ is the surface tension, θ the contact sample/mercury angle and P is the pressure. MIP has been applied to rigid solids that would resist to high pressure, and not chemically react with mercury.

2 MATERIALS AND METHODS

Samples from the cortical part of an adult bovine tibia bone were prepared by cutting 3 cm sample (Figure 1.a) which were washed, heated, and treated (up 60 °C) to facilitate the cleaning process. Then it was treated in a low aqueous solution concentration of sodium hypochlorite for one day to remove grease and gels from the pores (Figure 1.b). After this treatment, the samples were kept dry in an electric oven at 60 °C. In the MIP technique the bone sample immersed in mercury is subjected to increase isostatic pressure and the equipment register pairs of intrusion volume and pressure values. At the end of the intrusion cycle, the porosimeter starts the step of mercury extrusion through reduction of pressure. The equipment utilized was the Autopore II 9220, Micromeritics, with capacity to reach maximum isostatic pressure of 414 MPa and to measure pores in the range 3 nm - 360 µm. Experiments with cortical bone samples with all the sides free for mercury intrusion were repeated many times to check reproducibility of results.

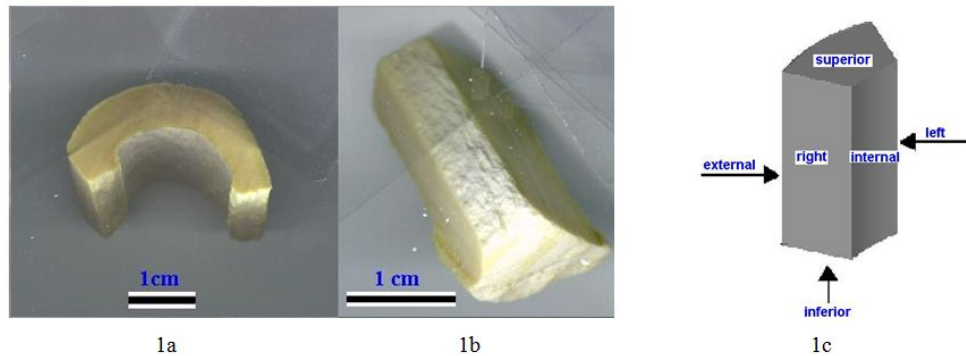


Figure 1: (a) Bovine tibia sample after treatment; (b) sealed shape sample; (c) Nomenclature used for the faces of the bone samples in the sealed faces MIP experiment.

To investigate from which sample face (Figure 1.c) the open pores have originated we have performed MIP experiments with sealed faces of the bone sample. Sealing has been accomplished by applying a commercial instantaneous glue film over the bone surface sample. To identify each side we have nominated the sides of the sample as indicated in Figure. 1.c. The software utilized for the pore structure visualization was VTK (Visualization Toolkit) [8, 9, 10] and the algorithms were written using the language TCL (Tool Command Language) [11, 12].

3 RESULTS AND DISCUSSION

Figure. 2.a presents SEM (scanning electron microscope) photomicrographs of the bovine tibia bone samples prior to MIP test and Figure 2.b SEM photomicrographs after mercury intrusion testing. The pore size concentration and distribution are presented in Figure 3 for a bone sample with all sides free for mercury intrusion. The area under the curve represents the concentration of the pores. The result indicates that a part of the cortical porosity is due to Havers and Volkmann canals. The graph also indicates that at least in the bovine tibia bone sample studied lacunae-caniculae porosity size distribution is narrower than the Havers/Volkmann porosity size distribution. The lacunae-caniculae porosity is concentrated around 0.1 µm. On the other hand, collagen-apatite porosity is only a small fraction of the total bone porosity volume. Mercury cumulative intrusion volume graph (Figure 4) shows the pore volume for each porosity type.

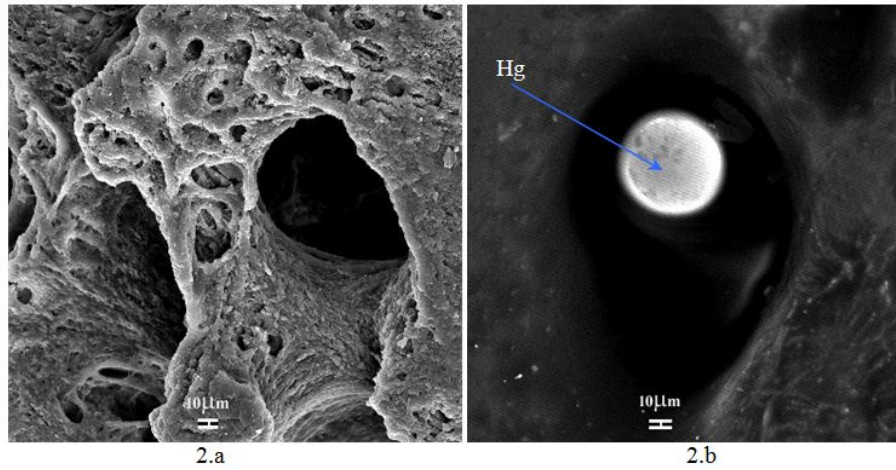


Figure 2: (a) SEM micrograph of the bone sample prior to MIP test. (b) SEM micrograph after mercury intrusion test. Bar: 10 microns.

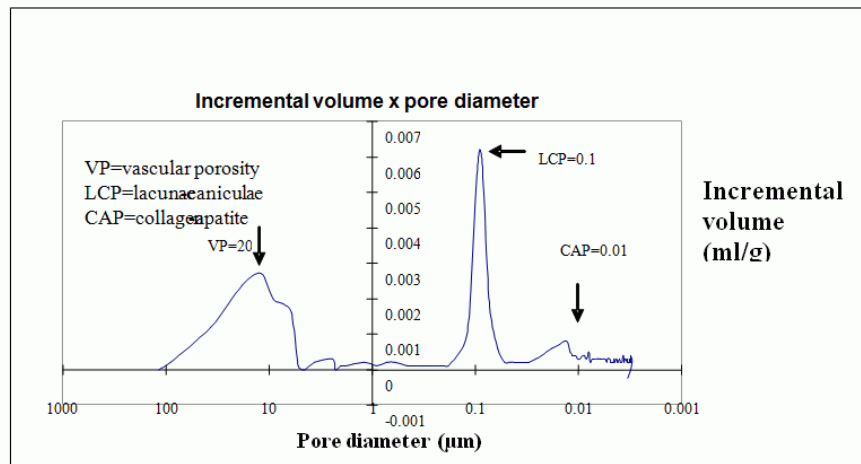


Figure 3: Incremental intrusion volume of mercury versus pore diameter.

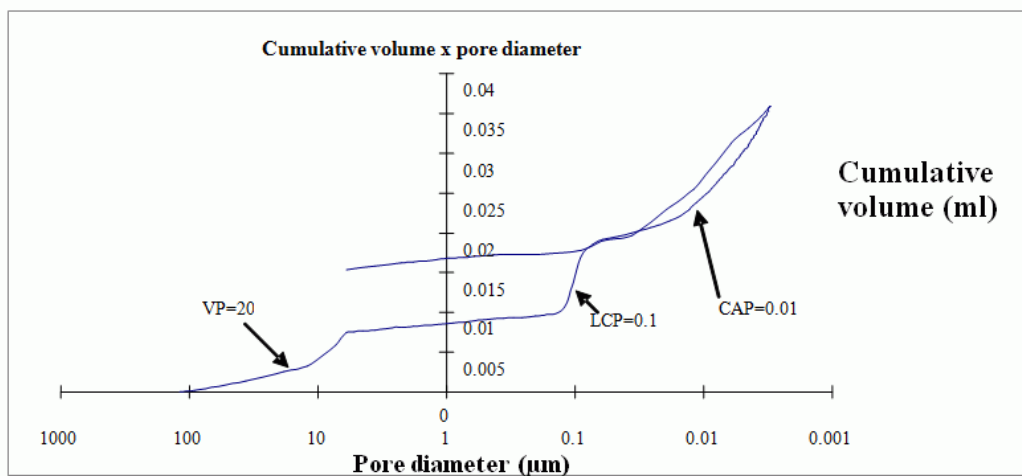


Figure 4: Mercury cumulative intrusion volume versus sample pore diameter with sides not sealed. VP = vascular porosity, LCP = lacunae – caniculae porosity and CAP = collagen – apatite porosity.

Table 1 displays which sample faces have been sealed (*cortical bone characteristics*) and the corresponding *Figure/Intrusion Curve*. No mercury intrusion occurred from sealed sides. Figures 6 and 7 present the results of MIP experiments with these sealed samples. Curve A (Figure 5) is from a sample with all but the superior and inferior sides sealed. In this case, mercury had been intruded on pore size range between 10 to 100 μm . This indicates that only Havers/Volkmann canals have been filled with mercury. Curve B (Figure 5) shows the result of the MIP experiment where only the internal and external sides of the cortical bone sample have been sealed. Mercury intrusion therefore occurred at the superior, inferior, right and left sides. Curve B has had intrusion in all the pore diameter types (canals, lacunae-caniculae and collagen-apatite porosity) and is similar to the intrusion curve of Figure. 4. Comparison between curve A and B indicates that lacunae-caniculae pores were not in contact with the superior and inferior sides of the cortical bone sample

Table 1: Cortical bone experiments with sealed sides

Experiment number	Figure/Intrusion Curve	Cortical bone sample characteristics
1	Figure 3	All sides free for mercury intrusion (no-sealed sides)
2	Figure 5 / Curve A	Only superior and inferior sample sides free for mercury intrusion
3	Figure 5 / Curve B	Only internal and external sample sides sealed
4	Figure 5 / Curve C	Only internal and external sample sides free for mercury intrusion
5	Figure 6 / Curve D	Only internal sample side free for mercury intrusion
6	Figure 6 / Curve E	Only external sample side free for mercury intrusion
7	Figure 6 / Curve F	Only right and left sample sides free for mercury intrusion

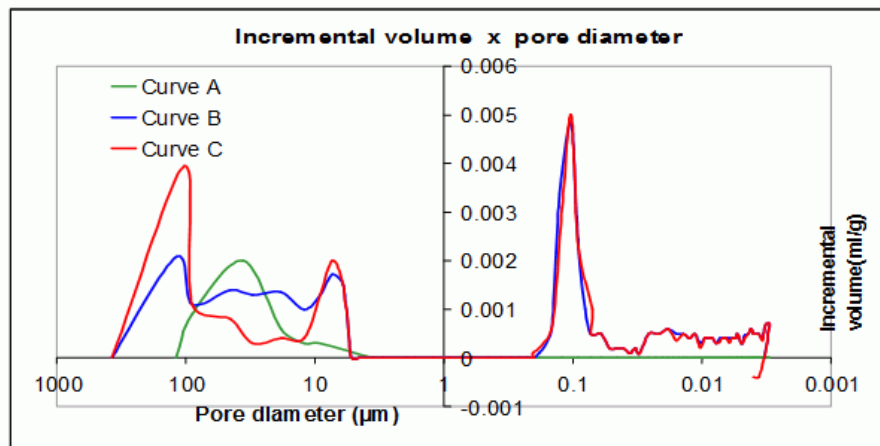


Figure 5: Incremental intrusion volume of mercury versus pore diameter

Curve C (Figure 5) shows the MIP experiment for a sample with the internal and external sides free for mercury intrusion and the other four sides glue-sealed. Curve D (Figure 6) is the intrusion curve where only the internal side was free for mercury intrusion. Curve E (Figure 6) is the experiment where only the external side was free for mercury intrusion. Finally, Curve F (Figure 6) is the result of the experiment with only the right and the left sides free for mercury intrusion.

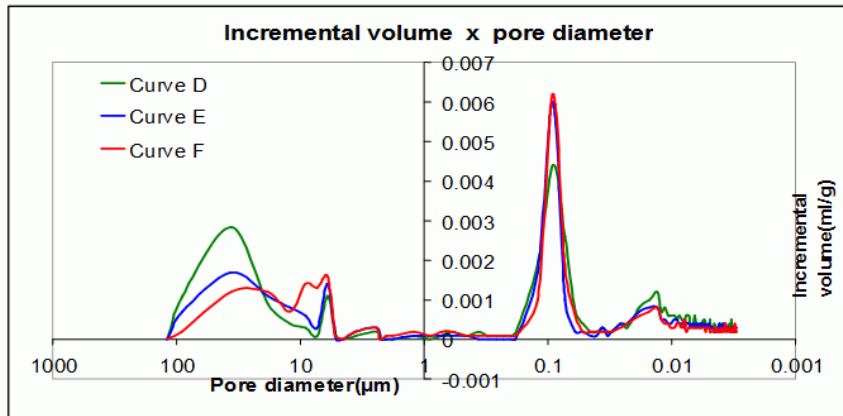


Figure 6: Incremental intrusion volume of mercury versus pore diameter

All curves display approximately the same porosity with the exception of curve A. Havers/Volkman vascular hollows seem to initiate at all six faces of the bovine tibia bone sample. The tested samples have indicated that the lacunae-caniculae system initiates from external and internal faces, as well as from right and left sides. However, there are no mercury intrusions into lacunae-caniculae porosity from superior and inferior bovine tibia bone sample sides. Further studies will be needed to test the hypothesis that caniculae and lacunae might be organized approximately in orthogonal planes to the Havers canals.

On the other hand, hysteresis is normally observed in porosimetry runs (see Figure 4) and it is associated with the contact angle change between the mercury intrusion and extrusion cycle. Figure 4 shows the extrusion curve close to the intrusion curve for pore sizes lower than 0.1 µm diameter. It seems that once the mercury has entered pores ≥ 0.1 µm it is retained there. One possible explanation is that these pores are caniculae.

Using MIP data (total porosity for each type) and knowing the mean pore diameter of vascular, lacunae, and the caniculae it was possible to calculate the volume occupied by each pore type in a (1. h = variable) mm³ unitary cell volume. Figure 7 presents the visualization of such a cylinder shaped cell of the porous structure of the bovine tibia sample. In this visualization the vascular and lacunae-caniculae porosity form one Havers system. The vascular porosity shows a central cylinder, one Havers canal. The lacunae-caniculae porosity is represented by ellipsoids (lacunae) and by very small cylinders (caniculae). Due to the scale of the structure cylinders appear as lines.

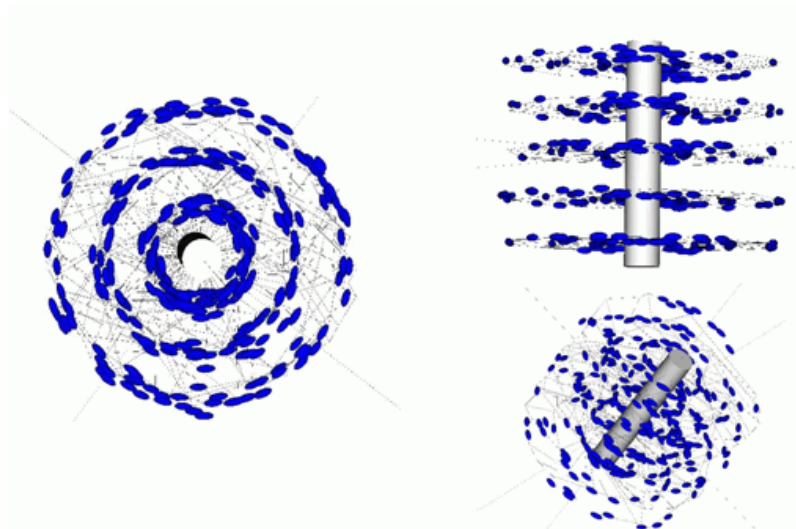


Figure 7: Three views of one Havers system using VTK software and MIP data. Dimensions of the cylinder shape unit cell: diameter = 0.32 mm; height (h) = variable; and volume = (1. h) mm³

4 CONCLUSIONS

Results confirm the effectiveness of the MIP technique in investigating the pore structure of the cortical bone material. MIP experiments associated with application of the VTK software for visualization seem to be a promising tool in the clarification of some aspects of bone porosity growth and especially the bone loss phenomenon.

5 BIBLIOGRAPHY

- [1] NYMANA, J.S., REYES, M., WANG, X., “Effect of ultrastructural changes on the toughness of bone”, *Micron*, v. 36, pp. 566-582, 2005.
- [2] COWIN, S.C., “Bone poroelasticity”, *Journal of Biomechanics*, v. 32, n. 3, pp. 217-238, 1999.
- [3] HAM, A.W., *Histologia (transl.)*, 2 ed, Rio de Janeiro, Guanabara Koogan S.A, 1977.
- [4] COSTA, L.F., OLIVEIRA, M.C.F., MINGHIM, R., “De olho nos Neurônios: as formas virtuais do pensamento”, *Ciência Hoje, Brasil*, v. 28-167, pp. 44 - 51, 01 mar. 2000.
- [5] WEBB, P.A., ORR, C., *Analytical Methods in Fine particle Technology*, 1 ed., Micromeritics Instrument Corp, Norcross, 1997.
- [6] AUTO-PORE II 9220, *Operator’s Manual*, Norcross, Micromeritics Instrument Corp, 1990.
- [7] WEBB, P.A., “An introduction to the physical characterization of materials by mercury intrusion porosimetry with emphasis on reduction and presentation of experimental data”, *Micromeritics Instrument Corp*, Norcross, 2001.
- [8] SCHROEDER, W.J., AVILA, L.S., HOFFMAN, W., “Visualizing with VTK: A Tutorial”, *IEEE Computer Graphics and Applications*, v. 20, n. 5, pp. 20-27, Sep./Oct., 2000.
- [9] SCHROEDER, W.J., MARTIN, K., LORENSEN, B., *The Visualization Toolkit: An Object-Oriented Approach To 3D*, 1 ed. New Jersey, Graphics, Prentice-Hall, 1996.
- [10] “THE VISUALIZATION TOOL KIT”, Available in: <http://public.kitware.com/VTK/>, Accessed: 05 October 2007.
- [11] “TCL and TK made easy”, Available in: <http://www.csc.calpoly.edu/~dbutler/tutorials/winter96/tcl/>, Accessed: 05 October 2007.
- [12] PAPADEMETRIS, X., *Introduction to Programming for Image Analysis with VTK*, Draft ed., Yale University, 2006. Available in: <http://www.bioimagesuite.org/vtkbook/xpvtkbook.pdf>, Accessed: 05 October 2007.